Measuring Cosmological Parameters with Cosmic Microwave Background Experiments

J. Richard Bond,[1] Robert Crittenden,[2] Richard L. Davis,[2] George Efstathiou,[3] and Paul J. Steinhardt[2]
[1]*Canadian Institute for Theoretical Astrophysics, University of Toronto, Toronto, Ontario, Canada M5S 1A7*
[2]*Department of Physics, University of Pennsylvania, Philadelphia, Pennsylvania 19104*
[3]*Department of Physics, Oxford University, Oxford, England OX1 3RH*
(Received 13 September 1993)

The cosmic microwave background anisotropy is sensitive to the slope and amplitude of primordial energy density and gravitational wave fluctuations, the baryon density, the Hubble constant, the cosmological constant, the ionization history, etc. In this Letter, we examine the degree to which these factors can be separately resolved from combined small- and large-angular-scale anisotropy observations. We isolate directions of degeneracy in this cosmic parameter space, but note that other cosmic observations can break the degeneracy.

PACS numbers: 98.80.Cq, 98.70.Vc, 98.80.Es

The observation of large-angular-scale ($\sim 10°$) fluctuations in the cosmic microwave background (CMB) [1,2] marks the beginning of a new age of precision measurement in cosmology [3–10]. Dramatic improvements in large- and small-angular-scale ($\lesssim 1°$) experiments [3–10] are anticipated. In this Letter, we explore the degree to which the CMB anisotropy observations can determine cosmological parameters such as the slope of the initial power spectrum, the age of the Universe, and the cosmological constant. We find that CMB anisotropy measurements alone cannot fix the parameters individually; however, a nontrivial combination of them can be determined. More concretely, for models based on the generation of Gaussian, adiabatic fluctuations by inflation, we have identified a new variable $\tilde{n}_s$, a function of the basic parameters that can be fixed to great precision by CMB anisotropy observations. Distinct models with nearly the same value of $\tilde{n}_s$ cannot be discriminated by CMB data alone. In a likelihood analysis, this leads to error contours centered around a highly elongated maximum-likelihood surface inside which $\tilde{n}_s$ is approximately constant. However, combined with other cosmological observations, determining $\tilde{n}_s$ is a powerful tool for testing models and measuring fundamental parameters.

We parametrize the space by

$$(C_2^{(S,T,Is,\ldots)},\ n_{s,t,is,\ldots},\ h,\ \Omega_B,\ \Omega_\Lambda, \Omega_{\rm CDM},\ \Omega_{\rm HDM}, \ldots)\ ,$$

where $H_0 = 100h\,{\rm km\,sec^{-1}\,Mpc^{-1}}$ is the Hubble parameter, and $\Omega_{B,\Lambda,{\rm CDM},{\rm HDM},\ldots}$ are the energy densities associated with baryons, cosmological constant (Λ), cold and hot dark matter, etc., divided by the critical density. We use the CMB quadrupole moments $C_2^{(S,T,Is,\ldots)}$ to parametrize the overall amplitudes of energy density (scalar metric), gravitational wave (tensor metric), isocurvature scalar, and other primordial fluctuations predicted by the model. We parametrize the shape of the initial (e.g., postinflation) fluctuation spectra in wave number k by power law indices $n_{s,t,is,\ldots}$, defined at time t_i by $k^3\langle|\widetilde{(\delta\rho/\rho)}(k,t_i)|^2\rangle \propto k^{n_S+3}$ and $k^3\langle|\tilde{h}_{+,\times}(k,t_i)|^2\rangle \propto k^{n_T}$, where $\delta\rho/\rho$ and $h_{+,\times}$ are the amplitudes of the energy density and gravitational wave metric fluctuations (for two polarizations), respectively.

In this Letter, we restrict ourselves to subdomains of this large space consistent with inflation models of fluctuation generation. Inflation produces a flat universe, $\Omega_{\rm total} \approx 1$. We also take $\Omega_{\rm HDM} = 0$, but note that, for angular scales $\gtrsim 10'$, the anisotropy for mixed dark matter models with $\Omega_{\rm CDM} + \Omega_{\rm HDM} \approx 1$ is quite similar to the anisotropy if all of the dark matter is cold. Given Ω_B, we impose the nucleosynthesis estimate [11,12] $\Omega_B h^2 = 0.0125$, to determine h; we also satisfy globular cluster and other age bounds [13], and gravitational lens limits [14]: we range from $h \lesssim 0.65$ for $\Omega_\Lambda = 0$ to $h \lesssim 0.88$ for $\Omega_\Lambda \lesssim 0.6$ [13,14].

Inflation produces adiabatic scalar [15] and tensor [16] Gaussian fluctuations. The quadrupole measured by the Cosmic Background Explorer (COBE) fixes $C_2^{(T)} + C_2^{(S)}$, but the tensor-to-scalar quadrupole ratio $r \equiv C_2^{(T)}/C_2^{(S)}$ is undetermined (e.g., see Fig. 1 in [17]). The indices n_s and n_t are determined by power-law best fits to the theoretical prediction over the scales probed by the CMB. For generic models of inflation, including new, chaotic, and extended models, inflation gives [17–19]

$$n_t \approx n_s - 1 \ \text{ and } \ r \equiv C_2^{(T)}/C_2^{(S)} \approx 7(1 - n_s)\ . \qquad (1)$$

Measuring r and n_s to determine whether they respect Eq. (1) is a critical test for inflation [20]. With this set of assumptions, we have reduced the parameter space to three dimensions, $(r|n_s, h, \Omega_\Lambda)$ (where $\Omega_B = 0.0125h^{-2}$ and $\Omega_{\rm CDM} = 1 - \Omega_B - \Omega_\Lambda$). We explicitly display both r and n_s but with a | as a reminder that r is determined by Eq. (1) given n_s; we have also assumed $n_t = n_s - 1$.

Our results are based on numerical integration of the general relativistic Boltzmann, Einstein, and hydrodynamic equations for both scalar [21] and tensor metric fluctuations using methods reported elsewhere

0031-9007/93/72(1)/13(4)$06.00

[19]. Included in the dynamical evolution are all the relevant components: baryons, photons, dark matter, and massless neutrinos. The temperature anisotropy, $\Delta T/T\,(\theta,\phi) = \sum_{\ell m} a_{\ell m} Y_{\ell m}(\theta,\phi)$, is computed in terms of scalar and tensor multipole components, $a_{\ell m}^{(S)}$ and $a_{\ell m}^{(T)}$, respectively. For inflation, each multipole for the two modes is predicted to be statistically independent and Gaussian distributed, fully specified by angular power spectra, $C_\ell^{(S)} = \langle |a_{\ell m}^{(S)}|^2 \rangle$ and $C_\ell^{(T)} = \langle |a_{\ell m}^{(T)}|^2 \rangle$.

Our results are presented in a series of two-panel figures (e.g., see Fig. 1). The upper plots show the spectrum C_ℓ's normalized to COBE, and the lower bar charts show the predicted $(\Delta T/T)_{\rm rms}$ for idealized experiments spanning 10° to 2′. The bar chart is constructed by computing $\langle (\Delta T/T)^2 \rangle = \frac{1}{4\pi}\sum (2\ell+1) C_\ell W_\ell$, where W_ℓ is a filter function that quantifies experimental sensitivity [19,22]. Errors arise from experimental noise and the theoretical cosmic variance. The error bars represent cosmic variance alone assuming full-sky coverage, exemplifying the limiting resolution achievable with CMB experiments. For more realistic error bars, consider a detection obtained from measurements $(\overline{\Delta T/T})_i \pm \sigma_D$ (where σ_D represents detector noise) at $i = 1, \ldots, N_D$ experimental patches sufficiently isolated from each other to be largely uncorrelated. For large N_D, the likelihood function falls by $e^{-\nu^2/2}$ from a maximum at $(\Delta T/T)_{\rm max}$ when

$$\left(\frac{\Delta T}{T}\right)^2 = \left(\frac{\Delta T}{T}\right)^2_{\rm max} \pm \sqrt{\frac{2}{N_D}}\,\nu \left[\left(\frac{\Delta T}{T}\right)^2_{\rm max} + \sigma_D^2\right]. \tag{2}$$

An experimental noise σ_D below 10^{-5} is standard now, and a few times 10^{-6} is soon achievable; hence if systematic errors and unwanted signals can be eliminated, the 1-sigma ($\nu = 1$) relative uncertainty in $\Delta T/T$ will be from cosmic variance alone, $1/\sqrt{2N_D}$, falling below

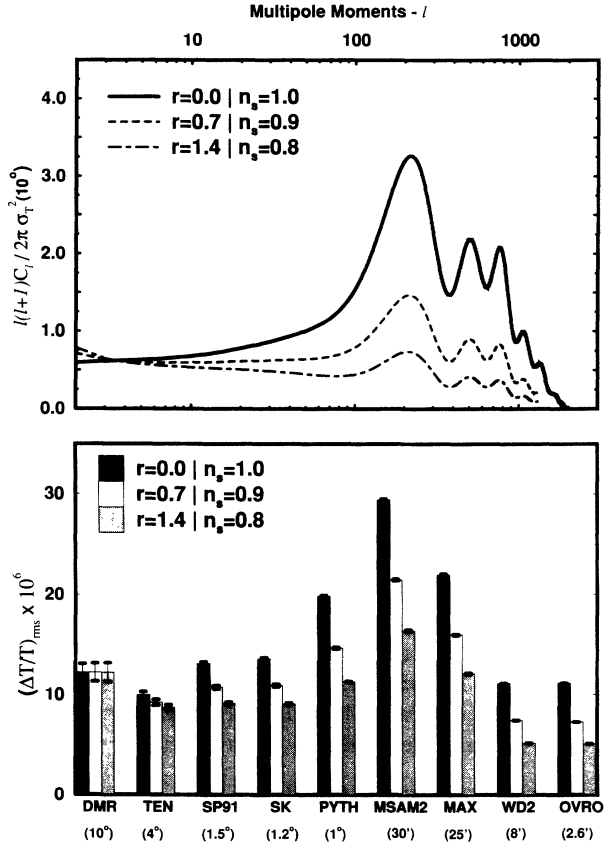

FIG. 1. Top: Power spectra as a function of multipole moment ℓ for (r=0|n_s=1), (r=0.7|n_s=0.9), and (r =1.4|n_s=0.8) where $h = 0.5$ and $\Omega_\Lambda = 0$ for all models. The spectra in all figures are normalized by the COBE $\sigma_T^2(10°) \equiv (4\pi)^{-1}\sum (2\ell+1) C_l \exp[-\ell(\ell+1)/158.4]$ (a Gaussian filter with 10° FWHM), observed by DMR to be $\sim 1.2 \times 10^{-10}$, with about a 30% error. Bottom: $(\Delta T/T)_{\rm rms}$ levels with 1-sigma cosmic variance error bars for nine experiments assuming full-sky coverage; see also Eq. (2). The Gaussian coherence angle is indicated below each experiment; see Refs. [1–11] for acronyms.

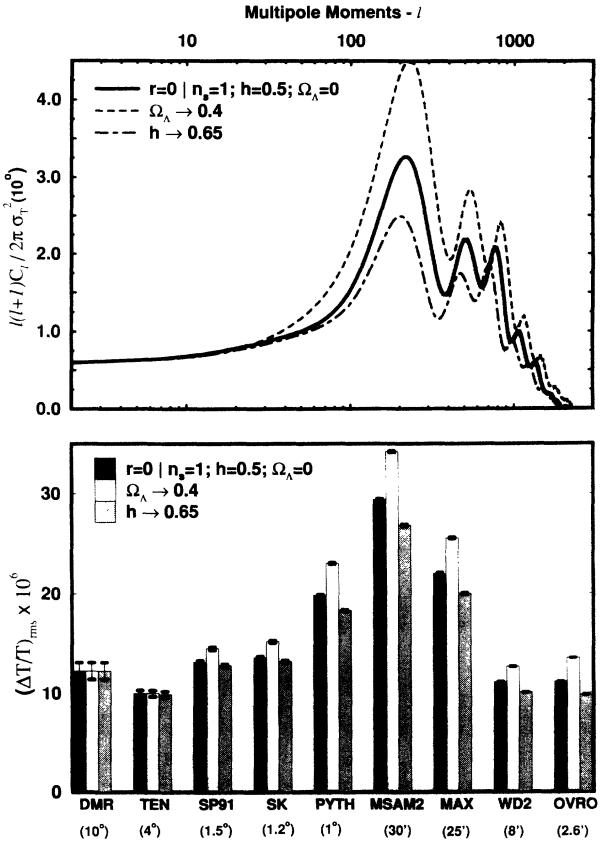

FIG. 2. Power spectra as a function of ℓ for scale-invariant models, with $r = 0|n_s = 1$. The middle curve shows $h = 0.5$ and $\Omega_\Lambda = 0$. In the upper curve, Ω_Λ is increased to 0.4 while keeping $h = 0.5$. In the lower curve, $\Omega_\Lambda = 0$ but h is increased from 0.5 to 0.65 (hence Ω_B drops from 0.5 to 0.3). The spectra are insensitive to changes in h for fixed Ω_B. Increasing Ω_Λ or Ω_B increases the power at $\ell \sim 200$.

10% for $N_D > 50$. The optimal variances shown in the figures roughly correspond to filling the sky with patches separated by $2\theta_{\rm FWHM}$.

Figure 1 shows how the small-angular signal is increasingly suppressed as r increases and n_s decreases [17,19]. For large maps, cosmic variance is significant for large-angle experiments [23], but shrinks to insignificant levels at smaller scales. It appears that $r|n_s$ could be resolved if Λ, h, and ionization history were known.

Figure 2 shows the effects of varying Ω_Λ or H_0 compared to our baseline (solid line) spectrum ($r = 0|n_s = 1, h = 0.5, \Omega_\Lambda = 0$). Increasing Ω_Λ (or decreasing h) enhances small-angular-scale anisotropy by reducing the redshift $z_{\rm eq}$ at which radiation-matter equality occurs. Increasing Ω_Λ also changes slightly the spectral slope for $\ell \lesssim 10$ due to Λ suppression of the growth of scalar fluctuations [24]. The bar chart shows that either $r|n_s$, Ω_Λ, or h can be resolved if the other two parameters are known.

A degree of "cosmic confusion" arises, though, if $r|n_s$, Ω_Λ, and h vary simultaneously. Figure 3 shows spectra for models lying in a two-dimensional surface of $(r|n_s, h, \Omega_\Lambda)$ which produce nearly identical spectra. In one case, $r|n_s$ is fixed, and increasing Ω_Λ is nearly compensated by increasing h. In the second case, h is fixed, but increasing Ω_Λ is nearly compensated by decreasing n_s [25].

Further cosmic confusion arises if we also consider ionization history [26]. Let z_R be the redshift at which we suppose sudden, total reionization of the intergalactic medium. Figure 4 compares spectra with standard recombination (SR), no recombination (NR), and late reionization (LR) at $z_R = 50$, where $h = 0.5$ and $\Omega_\Lambda = 0$. NR represents the behavior if reionization occurs early ($z_R \gg 200$). The spectrum is substantially suppressed for $\ell \gtrsim 200$ compared to any SR models. Experiments at $\lesssim 0.5°$ scale can clearly identify NR or early reionization ($z_R \gtrsim 150$ gives qualitatively similar results to NR). Reionization for $20 \lesssim z_R \lesssim 150$ results in modest suppression at $\ell \approx 200$, which can be confused with a

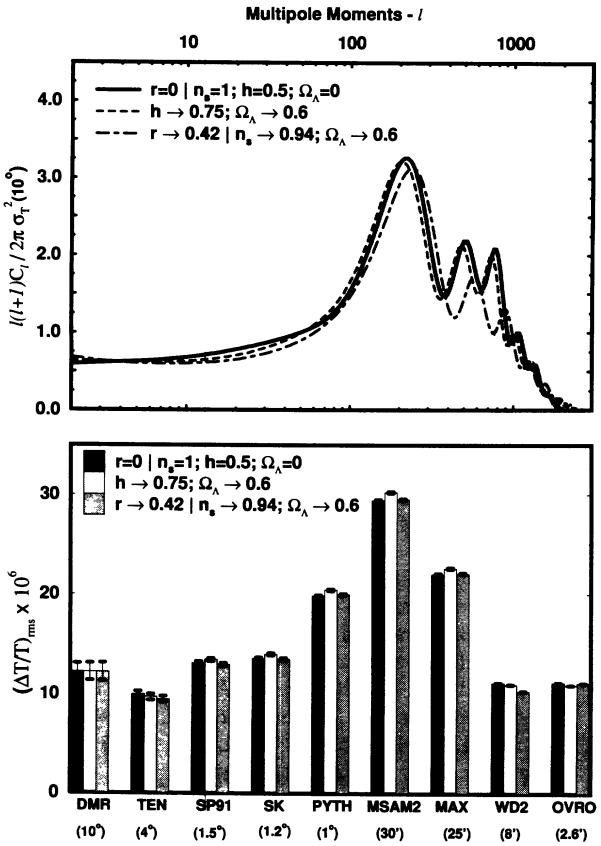

FIG. 3. Examples of different cosmologies with nearly identical spectra of multipole moments and $(\Delta T/T)_{\rm rms}$. The solid curve is $(r = 0|n_s = 1, h = 0.5, \Omega_\Lambda = 0)$. The other two curves explore degeneracies in the $(r = 0|n_s = 1, h, \Omega_\Lambda)$ and $(r|n_s, h = 0.5, \Omega_\Lambda)$ planes. In the dashed curve, increasing Ω_Λ is almost exactly compensated by increasing h. In the dot-dashed curve, the effect of changing to $r = 0.42|n_s = 0.94$ is nearly compensated by increasing Ω_Λ to 0.6.

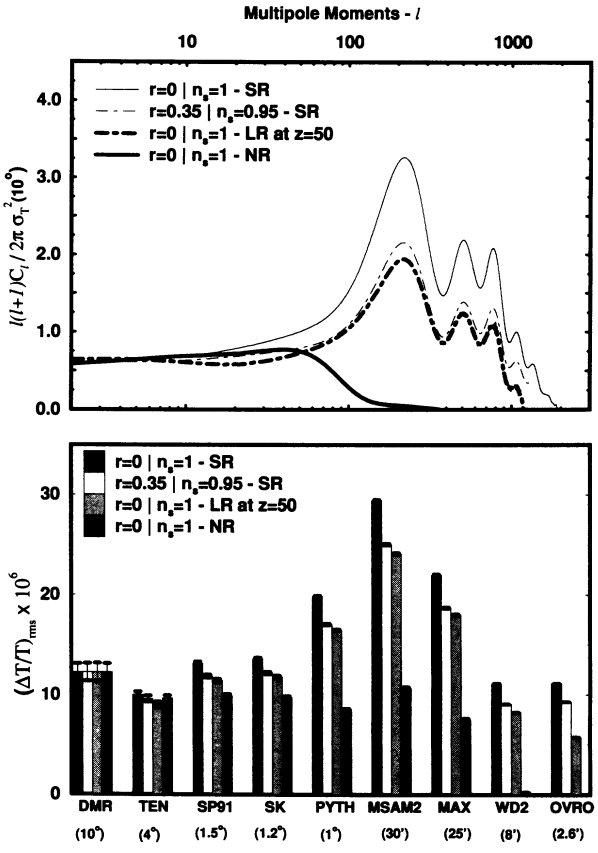

FIG. 4. Power spectra for models with standard recombination (SR), no recombination (NR), and "late" reionization (LR) at $z = 50$. In all models, $h = 0.5$ and $\Omega_\Lambda = 0$. NR or reionization at $z \geq 150$ results in substantial suppression at $\ell \geq 100$. Models with reionization at $20 \leq z \leq 150$ give moderate suppression that can mimic decreasing n_s or increasing h; e.g., compare the $n_s = 0.95$ spectrum with SR (thin, dot-dashed) to the $n_s = 1$ spectrum with reionization at $z = 50$ (thick, dot-dashed).

decrease in n_s (see figure).

The results can be epitomized by some simple rules of thumb: Over the $30' - 2°$ range, $(\Delta T/T)^2_{\rm rms}$ is roughly proportional to the maximum of $\ell(\ell+1)C_\ell$ (the first Doppler peak). Since the maximum (corresponding to $\sim 0.5°$ scales) is normalized to COBE differential microwave radiometer (DMR) measurements (at $\sim 10°$), its value is exponentially sensitive to n_s. Since scalar fluctuations account for the maximum, the maximum decreases as r increases. The maximum is also sensitive to the redshift at matter-radiation equality [or, equivalently, $(1-\Omega_\Lambda)h^2$], and to the optical depth at last scattering for late-reionization models, $\sim z_R^{3/2}$. These observations are the basis of an empirical formula (accurate to $\lesssim 15\%$)

$$\left.\frac{\ell(\ell+1)C_\ell}{2\pi\sigma_T^2(10°)}\right|_{\rm max} \approx A\, e^{B\,\tilde{n}_s}, \tag{3}$$

where $A = 0.1$, $B = 3.56$, and

$$\begin{aligned}\tilde{n}_s \approx\ & n_s - 0.28\ln(1+0.8r) \\ & -0.52[(1-\Omega_\Lambda)h^2]^{\frac{1}{2}} - 0.000\,36\, z_R^{3/2} + 0.26\,,\end{aligned} \tag{4}$$

where r and n_s are related by Eq. (1) for generic inflation models, and $z_R \lesssim 150$ is needed to have a local maximum ($\tilde{n}_s$ has been defined such that $\tilde{n}_s = n_s$ for $r = 0$, $h = 0.5$, $\Omega_\Lambda = 0$, and $z_R = 0$) [12]. Hence, the predicted anisotropy for any experiment in the range $10'$ and larger is not separately dependent on n_s, r, Ω_Λ, etc.; rather, it is a function of the combination $\tilde{n}_s$.

Our central result is that CMB anisotropy experiments can determine $\tilde{n}_s$, but variations of parameters along the surface of constant $\tilde{n}_s$ produce indistinguishable CMB anisotropy. Given present uncertainties in h, Ω_Λ, and z_R, it will be possible to determine the true spectral index n_s (or r) to within 10% accuracy using the CMB anisotropy alone. Quantitative improvement can be gained by invoking constraints from large-scale structure, e.g., galaxy velocity and cluster distributions, although the results are model dependent. Ultimately, tighter limits on Ω_Λ, h, ionization history, and the dark matter density are needed before the CMB anisotropy can develop into a high precision test of inflation.

This research was supported by the DOE at Penn (DOE-EY-76-C-02-3071), NSERC at Toronto, the SERC at Oxford, and the Canadian Institute for Advanced Research.

[1] DMR, G.F. Smoot *et al.*, Astrophys. J. Lett. **396**, L1 (1992).
[2] K. Ganga *et al.*, Astrophys. J. **410**, L57 (1993).
[3] MSAM (2-beam), E. S. Cheng *et al.* (to be published).
[4] TEN, R.A. Watson *et al.*, Nature (London) **357**, 660 (1992).
[5] SP91 (South Pole 1991), T. Gaier *et al.*, Astrophys. J. Lett. **398**, L1 (1992); J. Schuster *et al.*, Astrophys. J. Lett. **412**, L47 (1993).
[6] SK, E.J. Wollack, N.C. Jarosik, C.B. Netterfield, L.A. Page, and D. Wilkinson, Princeton University report, 1993 (to be published).
[7] OVRO, A.C.S. Readhead *et al.*, Astrophys. J. **346,** 556 (1989).
[8] MAX, P. Meinhold *et al.*, Astrophys. J. Lett. **409**, L1 (1993); J. Gunderson *et al.*, Astrophys. J. Lett. **413**, L1 (1993).
[9] WD2 (White Dish), G.S. Tucker, G.S. Griffin, H. Nguyen, and J.B. Peterson, Princeton University report, 1993 (to be published).
[10] PYTHON, M. Dragovan *et al.* (private communication).
[11] T.P. Walker, G. Steigman, D.N. Schramm, K.A. Olive, and H.S. Kang, Astrophys. J. **376**, 51 (1991).
[12] In a forthcoming paper, we show how increasing $\Omega_B h^2$ increases the Doppler peak and changes the spectral shape.
[13] E.W. Kolb and M. S. Turner, *The Early Universe* (Addison-Wesley, Redwood City, CA, 1990).
[14] D. Maoz and H.-W. Rix, Astrophys. J. (to be published).
[15] J. Bardeen, P. J. Steinhardt, and M. S. Turner, Phys. Rev. D **28**, 679 (1983); A. H. Guth and S.-Y. Pi, Phys. Rev. Lett. **49**, 1110 (1982); A. A. Starobinsky, Phys. Lett. **117B**, 175 (1982); S. W. Hawking, Phys. Lett. **115B**, 295 (1982).
[16] V. A. Rubakov, M. V. Sazhin, and A. V. Veryaskin, Phys. Lett. **115B**, 189 (1982); L.F. Abbott and M. Wise, Nucl. Phys. **B244**, 541 (1984); A.A. Starobinsky, Pis'ma Astron. Zh. **11**, 323 (1985) [Sov. Astron. Lett. **11**, 133 (1985)].
[17] R.L. Davis, H.M. Hodges, G.F. Smoot, P.J. Steinhardt, and M.S. Turner, Phys. Rev. Lett. **69**, 1856 (1992).
[18] F. Lucchin, S. Matarrese, and S. Mollerach, Astrophys. J. Lett. **401**, 49 (1992); D. Salopek, Phys. Rev. Lett. **69**, 3602 (1992); A. Liddle and D. Lyth, Phys. Lett. B **291**, 391 (1992); V. Sahni and T. Souradeep, Mod. Phys. Lett. A **7**, 3541 (1992); J.E. Lidsey and P. Coles, Mon. Not. R. Astron. Soc. **258**, 57P (1992); F.C. Adams, J.R. Bond, K. Freese, J.A. Frieman, and A.V. Olinto, Phys. Rev. D **47**, 426 (1993).
[19] R. Crittenden, J.R. Bond, R.L. Davis, G. Efstathiou, and P.J. Steinhardt, Phys. Rev. Lett. **71**, 324 (1993); numerical methods are discussed in a forthcoming paper.
[20] Exceptions to Eq. (1) require *additional* fine tuning of parameters or initial conditions, beyond that which is strictly necessary for inflation. Examples include cosine potentials ("natural inflation") or potentials in any inflationary model in which an extremum or discontinuity is encountered near the end of inflation. Note that Eq. (4) shows dependence on r and n_s separately, and is thus valid for the exceptional models as well.
[21] J.R. Bond and G. Efstathiou, Astrophys. J. **285**, L45 (1984); Mon. Not. R. Astron. Soc. **226**, 655–687 (1987).
[22] J.R. Bond, G. Efstathiou, P.M. Lubin, and P. Meinhold, Phys. Rev. Lett. **66**, 2179 (1991).
[23] M. White, L. Krauss, and J. Silk, Yale Report No. YCTP-P44-92 (to be published).
[24] L. Kofman and A.A. Starobinsky, Pis'ma Astron. Zh. **11**, 643 (1985) [Sov. Astron. Lett. **11**, 271 (1985)].
[25] L. Kofman, N. Gnedin, and N. Bahcall, Astrophys. J. **413**, 1 (1993).
[26] Inflation-based models are likely to have negligibly small z_R [21]; the large z_R examples shown here suggest the small-angular-scale suppression characteristic of models which require large z_R (e.g., cosmic strings and textures).

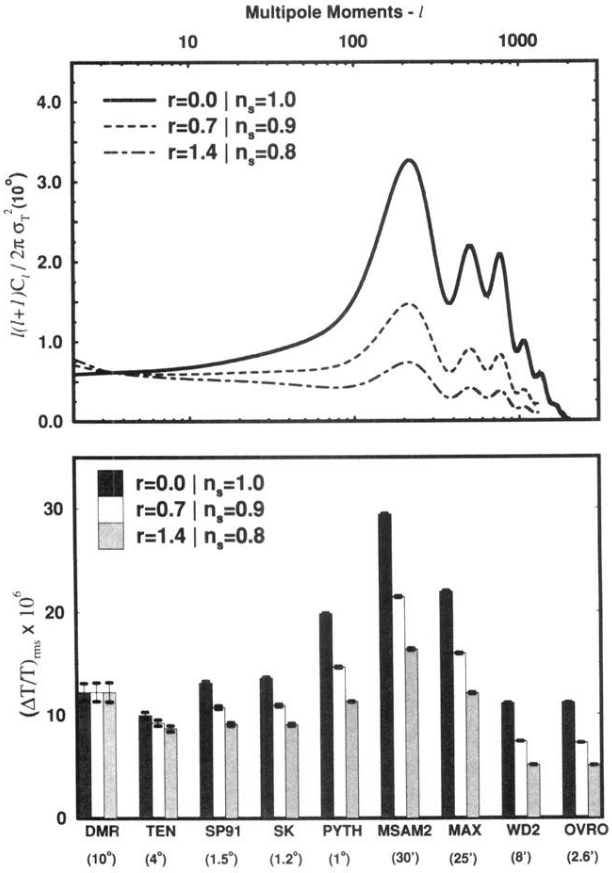

FIG. 1. Top: Power spectra as a function of multipole moment ℓ for (r=0|n_s=1), (r=0.7|n_s=0.9), and (r =1.4|n_s=0.8) where $h = 0.5$ and $\Omega_\Lambda = 0$ for all models. The spectra in all figures are normalized by the COBE $\sigma_T^2(10^\circ) \equiv (4\pi)^{-1}\sum(2\ell+1)C_l \exp[-\ell(\ell+1)/158.4]$ (a Gaussian filter with 10° FWHM), observed by DMR to be $\sim 1.2 \times 10^{-10}$, with about a 30% error. Bottom: $(\Delta T/T)_{\rm rms}$ levels with 1-sigma cosmic variance error bars for nine experiments assuming full-sky coverage; see also Eq. (2). The Gaussian coherence angle is indicated below each experiment; see Refs. [1–11] for acronyms.

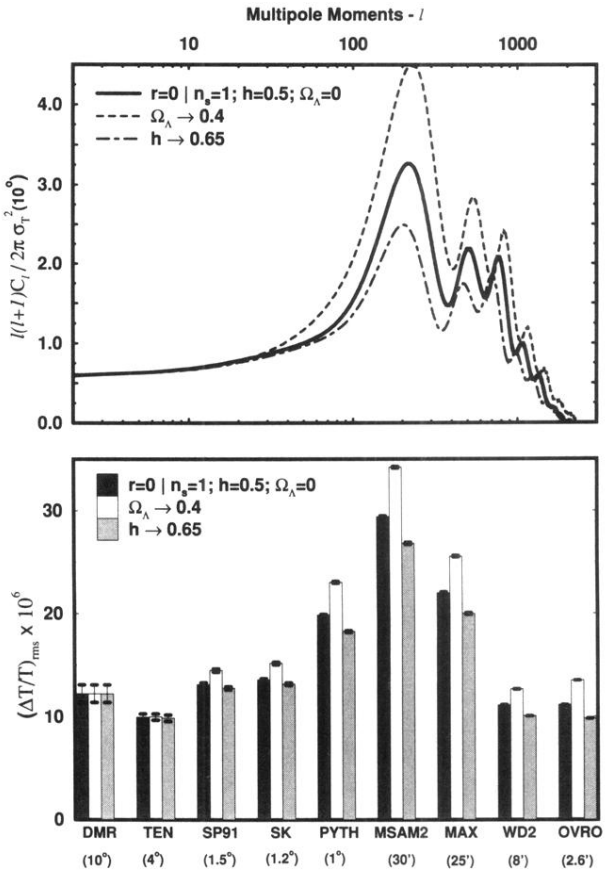

FIG. 2. Power spectra as a function of ℓ for scale-invariant models, with $r = 0|n_s = 1$. The middle curve shows $h = 0.5$ and $\Omega_\Lambda = 0$. In the upper curve, Ω_Λ is increased to 0.4 while keeping $h = 0.5$. In the lower curve, $\Omega_\Lambda = 0$ but h is increased from 0.5 to 0.65 (hence Ω_B drops from 0.5 to 0.3). The spectra are insensitive to changes in h for fixed Ω_B. Increasing Ω_Λ or Ω_B increases the power at $\ell \sim 200$.

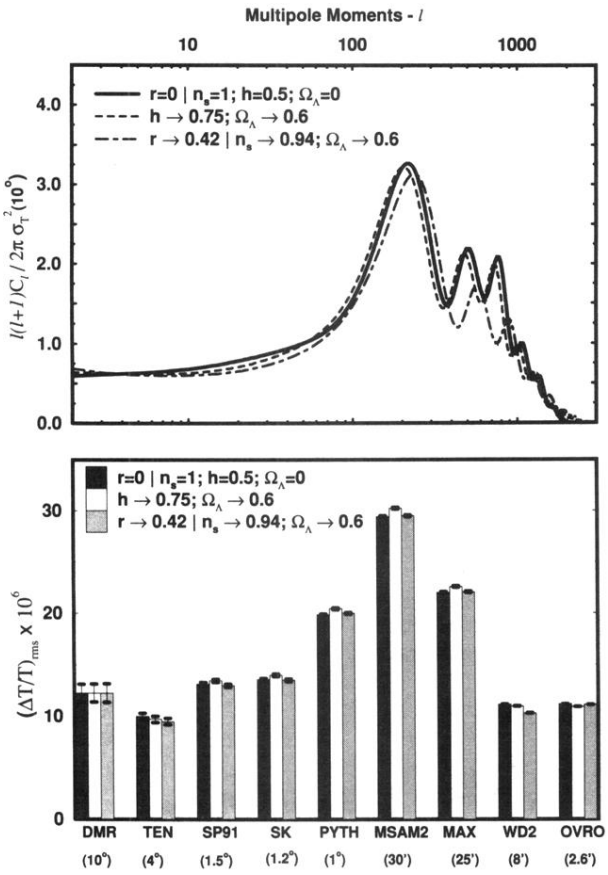

FIG. 3. Examples of different cosmologies with nearly identical spectra of multipole moments and $(\Delta T/T)_{\rm rms}$. The solid curve is $(r = 0|n_s = 1, h = 0.5, \Omega_\Lambda = 0)$. The other two curves explore degeneracies in the $(r = 0|n_s = 1, h, \Omega_\Lambda)$ and $(r|n_s, h = 0.5, \Omega_\Lambda)$ planes. In the dashed curve, increasing Ω_Λ is almost exactly compensated by increasing h. In the dot-dashed curve, the effect of changing to $r = 0.42|n_s = 0.94$ is nearly compensated by increasing Ω_Λ to 0.6.

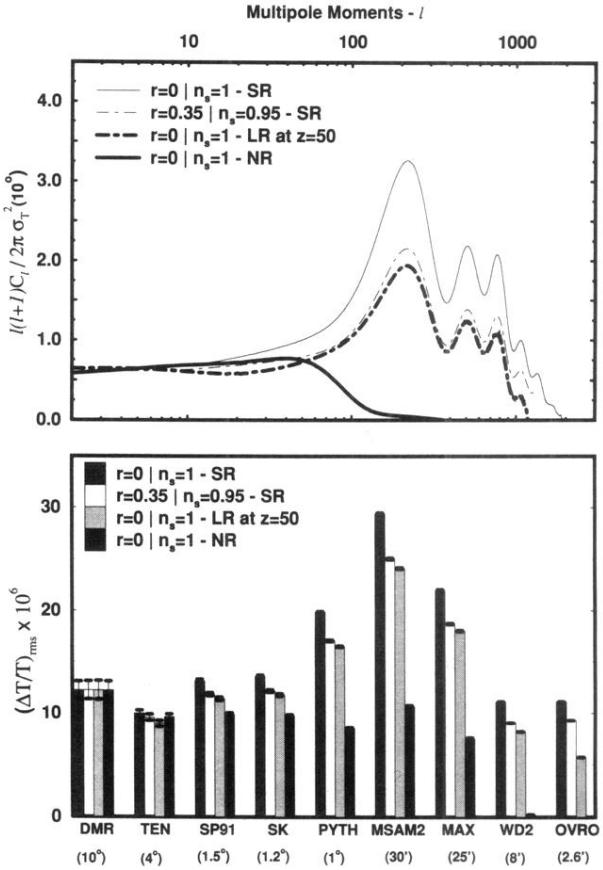

FIG. 4. Power spectra for models with standard recombination (SR), no recombination (NR), and "late" reionization (LR) at $z = 50$. In all models, $h = 0.5$ and $\Omega_\Lambda = 0$. NR or reionization at $z \geq 150$ results in substantial suppression at $\ell \geq 100$. Models with reionization at $20 \leq z \leq 150$ give moderate suppression that can mimic decreasing n_s or increasing h; e.g., compare the $n_s = 0.95$ spectrum with SR (thin, dot-dashed) to the $n_s = 1$ spectrum with reionization at $z = 50$ (thick, dot-dashed).